INTERNATIONAL JOURNAL FOR NUMERICAL METHODS IN FLUIDS, VOL. 3, 103–123 (1983)

NUMERICAL SOLUTIONS FOR SOLUTE TRANSPORT IN UNCONFINED AQUIFERS

V. GUVANASEN† AND R. E. VOLKER‡

Department of Civil and Systems Engineering, James Cook University of North Queensland, Q. 4811, Australia

SUMMARY

Two numerical methods for solving the problem of solute transport in unsteady flow in unconfined aquifers are studied. They are the method of characteristics (MOC) based on the finite difference method (FDM), and the finite element method (FEM). The FEM is further subdivided into four schemes: moving mesh, pseudo-Lagrangian (FEM1); stationary mesh, pseudo-Lagrangian (FEM2); pseudo saturated–unsaturated, Eulerian (FEM3); and non-stationary element, Eulerian (FEM4).

Experiments on a one-dimensional flow case are performed to illustrate the schemes and to determine the effect of discretization on accuracy. In two-dimensional flow the above methods are compared with experimental results from a sand box model. Results indicate that for a similar degree of accuracy, the FEM requires less computational effort than the MOC. Among the four FEM schemes, FEM4 appears to be most attractive as it is the most efficient and most convenient to apply.

KEY WORDS Aquifers Convection Dispersion Finite Difference Finite Element Mass Transport Numerical Solutions Unconfined Flow

INTRODUCTION

Problems of flow and solute transport in unconfined aquifers (see Figure 1) are often solved by the saturated–unsaturated approach.[1] Owing to the high degree of non-linearity in the flow equation, computation is usually very expensive and for problems where the transport in the unsaturated zone is insignificant, some analysts have considered only the saturated zone.[2,3] The flow equation then is linear and can be cheaply solved but the major drawback is the necessity to deal with the moving free surface or the non-stationary saturated domain (see Figure 1).

Numerous numerical solutions for flow problems with a moving free surface have been given by various workers,[4,5] some of which have been studied and compared recently by the authors.[6] Numerical solutions for transport problems with a moving free surface, on the other hand, have not been examined in detail. The major objective of this study is therefore to compare some of the available methods so that an appropriate selection may be made. The solution methods are drawn from both the finite difference method (FDM) and the finite element method (FEM).

In solving the transport equation (also referred to as the convective-dispersion equation or the hydrodynamic dispersion equation), numerical solutions can produce severe numerical errors especially when convective transport is dominant and a Eulerian co-ordinate system is used. These errors can take the form of numerical dispersion which produces spurious

† Research Scholar; now Staff Scientist, Earth Sciences Division, Lawrence Berkeley Laboratory, University of California, Berkeley, CA 94720, U.S.A.
‡ Associate Professor

0271–2091/83/020103–21$02.10

Received 3 July 1981
Revised 4 May 1982

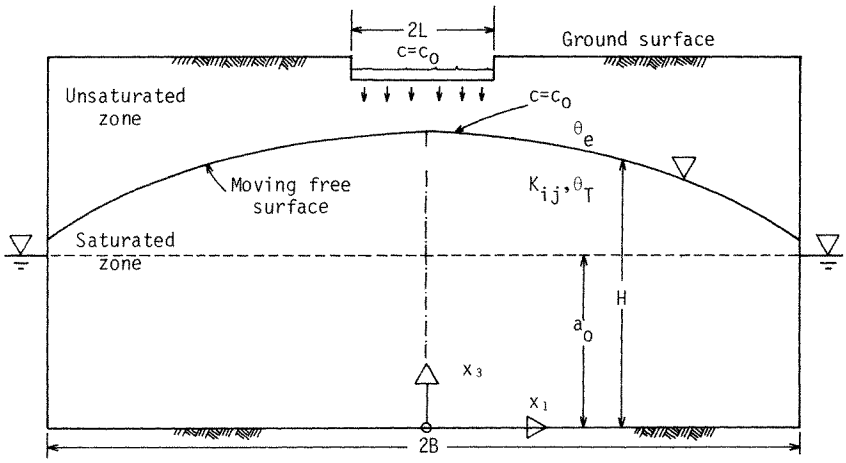

Figure 1. The solution domain in the unconfined aquifer

oscillation of the numerical solution about the true solution; in addition numerical diffusion can produce smearing of the front instead of a well defined sharp demarcation between the uncontaminated and contaminated water.

In an attempt to alleviate these problems many FDMs have been presented. The method of characteristics (MOC) which eliminates the convective terms and reduces the transport equation to a conduction equation was proposed by Garder *et al.*[7] and later refined by Reddell and Sunada.[8] Many other techniques have been employed such as selective one-sided difference approximations to the convective terms[9] and the flux corrected approach.[10]

In this study, MOC is selected because of its ability to deal with convection dominant problems and because, without the convective terms the Neumann type boundary conditions are relatively simple to incorporate at the curved moving free surface.

Numerical problems arise with the finite element solutions as they do with the FDM; however, FEM proves to be more stable than most FDM.[11] In an attempt to minimize the problem of numerical smearing and dispersion, some workers have applied asymmetric weighting (upwind) functions via the weighted residual method.[12] Alternatively, Hermitian basis functions have also been employed.

The upwind scheme, while reducing numerical dispersion, increases numerical diffusion, and the Hermitian elements improve accuracy at the expense of increased computational time and storage.

An alternative is to use a Lagrangian approach which has been applied successfully by several workers including Sato and Thomson.[13] This approach is well suited to the problem of a non-stationary free surface because of the manner in which the convection is introduced.

One Lagrangian approach is to allow for convection by moving the nodal points of the finite element mesh with the average pore velocity of the fluid in the vicinity of each node but difficulty may be encountered for complex flow problems in obtaining a well graded mesh. This difficulty can be overcome by an alternative scheme in which the convection is calculated by a backward-in-time interpolation scheme.

Two Eulerian schemes applicable to the moving free surface problems are also examined: the pseudo saturated–unsaturated approach and the non-stationary element approach.[3,14]

The accuracy and efficiency of these methods are determined by results from numerical experiments in a one-dimensional problem for which an analytical solution is available and in

two-dimensional problems for which some experimental data are available. Because there are many factors such as coding efficiency and program structure which must be taken into consideration when comparing various computer programs, results of run times of various schemes presented in this paper should be regarded as a guideline rather than an exact measurement.

MATHEMATICAL BACKGROUND

Flow equation

From the use of Darcy's law and the continuity condition, incompressible flow in rigid porous media can be tensorially expressed as[15]

$$\frac{\partial}{\partial x_i} K_{ij} \frac{\partial h}{\partial x_j} = 0, \qquad i = 1, 2, 3 \tag{1}$$

where K_{ij} is the hydraulic conductivity tensor, h the piezometric head, and x_i the Cartesian co-ordinates, x_3 being vertically upwards.

Boundary conditions are normally of the types below:

(i) Constant head boundary;

$$h = H_c$$

where H_c is the head on the boundary.

(ii) Prescribed flux boundary:

$$q_n = K_{ij} \frac{\partial h}{\partial x_j} l_i \tag{3}$$

where q_n is the flux normal to the boundary (positive inwards), and l_i the component of unit outward normal to the boundary.

(iii) Seepage surface:

$$h = x_3 \tag{4}$$

(iv) Free surface[5]

$$h = H = x_3 \tag{5a}$$

and

$$\left(P_0 - \theta_e \frac{\partial H}{\partial t}\right) l_3 = K_{ij} \frac{\partial h}{\partial x_j} l_i \tag{5b}$$

where θ_e is the effective porosity[15] at the free surface, P_0 the infiltration rate, H the elevation of the free surface above reference datum, and t the time.

Transport equation (hydrodynamic dispersion equation)

The hydrodynamic dispersion equation for incompressible flow is given by Bear[15] as

$$\frac{\partial c}{\partial t} + u_i \frac{\partial c}{\partial x_i} = \frac{\partial}{\partial x_i}\left(D'_{ij} \frac{\partial c}{\partial x_j}\right) \tag{6}$$

where c is the solute concentration, D'_{ij} the hydrodynamic dispersion coefficient tensor, and u_i the local pore velocity in the ith direction given by

$$u_i = -\frac{K_{ij}}{\theta_T} \frac{\partial h}{\partial x_j}$$

where θ_T is the Darcy porosity.

Boundary conditions are normally of the following types:

(i) Prescribed concentration:

$$c = c_b \tag{7}$$

where c_b is the concentration on the boundary.

(ii) Prescribed solute flux:

$$\theta_T l_i\left(-D'_{ij}\frac{\partial c}{\partial x_j} + u_i c\right) = \bar{\theta}_T l_i\left(-\bar{D}'_{ij}\frac{\partial \bar{c}}{\partial x_j} + \bar{u}_i \bar{c}\right) \tag{8a}$$

where terms with bars refer to variables outside the boundary of the saturated region.

This equation is reduced to

$$D'_{ij}\frac{\partial c}{\partial x_j} l_i = 0 \tag{8b}$$

for the case of an impermeable boundary.

(iii) Free surface[3,14]

$$\left(P_0 + \theta_{init}\frac{\partial H}{\partial t}\right)\frac{l_3}{\theta_T}(c - c_0) = -D'_{ij}\frac{\partial c}{\partial x_j} l_i \quad \text{for} \quad P_0 \neq 0, \quad \frac{\partial H}{\partial t} \geqslant 0, \tag{9a}$$

$$\frac{\theta_{init}}{\theta_T}\frac{\partial H}{\partial t} l_3(c - c_{ext}) = -D'_{ij}\frac{\partial c}{\partial x_j} l_i \quad \text{for} \quad P_0 = 0, \quad \frac{\partial H}{\partial t} \geqslant 0, \tag{9b}$$

and

$$-D'_{ij}\frac{\partial c}{\partial x_j} l_i = 0 \quad \text{for} \quad \frac{\partial H}{\partial t} < 0 \tag{9c}$$

where c_0 is the concentration of infiltrating solute, c_{ext} the concentration of immobile solute in the unsaturated zone above the free surface, θ_{init} the portion of pore space occupied by immobile solute in the unsaturated zone. Equations 9(a) and 9(b), in which terms on the left hand side represent convective flux per unit free surface area, are derived from the continuity condition at the free surface. Detailed derivations are given in References 3 and 14.

NUMERICAL SOLUTIONS

Various types of numerical solution to the flow equation have been given and discussed elsewhere[6] and are therefore not repeated in this paper. Five numerical solutions for the transport or hydrodynamic dispersion equation are investigated including one finite-difference scheme based on the method of characteristics (MOC), and four finite-element (FEM) schemes based on both Eulerian and Lagrangian formulations. For simplicity the following presentation is intended for two-dimensional problems although extension to three-dimensional cases is straightforward and does not involve any new concept.

Method of characteristics (MOC)

The details of this type of numerical model have been given by Garder *et al.*[7] and Reddell and Sunada[8] and are only briefly presented here.

Solutions to equation (6) may be obtained by solving the following set of simultaneous

differential equations.[7]

$$\frac{dx_i}{dt} = u_i \tag{10a}$$

$$\frac{dc}{dt} = \frac{\partial}{\partial x_i} D'_{ij} \frac{\partial c}{\partial x_j} \tag{10b}$$

The numerical procedure involves both a stationary grid and a set of moving points. The stationary grid is a conventional finite-difference grid and is normally the one employed for the flow equation solution.

The moving points are used to solve numerically equations (10a) and (10b). Each point represents one characteristic curve, and values of x, z, c are obtained as functions of t for each characteristic.

Each of the moving points is assigned a concentration which varies with time. At each time interval the moving points are relocated using a simple finite-difference form given by

$$x_{i_p}^{t+\Delta t} = x_{i_p}^{t} + u_{i_p}^{t+\Delta t} \Delta t \tag{11}$$

where x_{i_p} is the co-ordinate of the pth moving point, u_{i_p} the velocity of the pth moving point, and Δt the size of timestep. Each cell (see Figure 2) in the grid system is assigned a concentration equal to the average of the concentration of the moving points located inside the cell at time $t+\Delta t$. The concentration of the cell and each moving point inside the cell is then modified for dispersion by solving equation (10b) using an explicit-in-time, centred-in-space finite-difference approximation given by:

$$\frac{c_{I,J}^{t+\Delta t} - c_{I,J}^{t}}{\Delta t} = \Delta_i [D'_{ij} (\Delta_j c_{I,J}^{t})] \tag{12}$$

in which $c_{I,J}$ represents concentration at node (I, J), superscripts represent the time level, and Δ_i represent the spatial finite-difference approximation of $\partial/\partial x_i$.

The treatment of the free surface boundary condition is given in Guvansen[14] and details of computational procedure are given by Reddell and Sunada.[8]

An implicit scheme for equation (12) can also be formulated to remove the stability constraint associated with the explicit formulation. For problems in which dispersion coefficients are small, i.e. with sharp fronts, the explicit scheme is much more economical to employ than the implicit one.

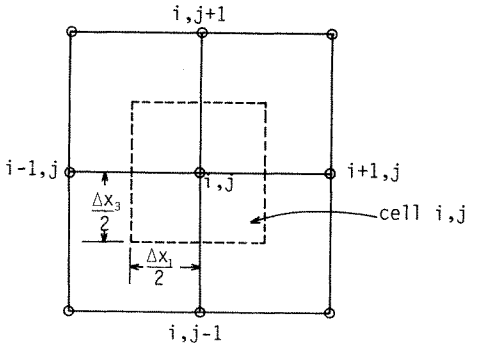

Figure 2. Stationary grid arrangement and a typical interior cell, MOC

Finite element method (FEM)

Let the solution be approximated in the form

$$c \simeq \hat{c} = c_I(t) N_I(x_i), \quad I = 1, 2, \ldots, \text{no. of connected nodes} \tag{13}$$

where repeated upper-case indices also indicate summation, and N_I is the interpolating function.

Applying the weighted residual method to equation (6) one obtains

$$\int_A W_I \left(\frac{\partial \hat{c}}{\partial t} + u_i \frac{\partial \hat{c}}{\partial x_i} - \frac{\partial}{\partial x_i} D'_{ij} \frac{\partial \hat{c}}{\partial x_j} \right) \mathrm{d}A = 0 \tag{14}$$

where W_I is the weighting function and A the area over which the integration takes place.

Using Green's theorem and equation (13), equation (14) becomes

$$\int_A \left(W_I N_J \frac{\mathrm{d}c_J}{\mathrm{d}t} + u_i W_I \frac{\partial N_J}{\partial x_i} c_J + D'_{ij} \frac{\partial W_I}{\partial x_i} \frac{\partial N_J}{\partial x_j} c_J \right) \mathrm{d}A - \int_S W_I D'_{ij} \frac{\partial \hat{c}}{\partial x_j} l_i \, \mathrm{d}S = 0 \tag{15}$$

which yields the following system of simultaneous equations

$$[M]\left\{\frac{\mathrm{d}c}{\mathrm{d}t}\right\} + [ST]\{c\} + \{F\} = 0 \tag{16}$$

where

$$M_{IJ} = \sum_e \int_A W_I N_J \, \mathrm{d}A$$

$$ST_{IJ} = \sum_e \int_A \left(W_I u_i \frac{\partial N_J}{\partial x_i} + D'_{ij} \frac{\partial W_I}{\partial x_i} \frac{\partial N_J}{\partial x_j} \right) \mathrm{d}A$$

$$F_I = \sum_e - \int_S W_I D'_{ij} \frac{\partial \hat{c}}{\partial x_j} l_i \, \mathrm{d}S$$

in which $\sum_e$ represents summation of elemental contributions and S is the boundary surface over which integration takes place. If $W_I = N_I$ in the above equation, the approach corresponds to the Galerkin technique.

Equation (16) is recast in the form

$$\left(\frac{[M]^{t+\Delta t}}{\Delta t} \{c\}^{t+\Delta t} - \frac{[M]^t}{\Delta t} \{c\}^t \right) + \lambda [ST]^{t+\Delta t} \{c\}^{t+\Delta t} + (1-\lambda)[ST]^t \{c\}^t + \lambda \{F\}^{t+\Delta t} + (1-\lambda)\{F\}^t = 0$$

which is rearranged to give

$$\left(\frac{[M]^{t+\Delta t}}{\Delta t} + \lambda [ST]^{t+\Delta t} \right) \{c\}^{t+\Delta t} - \left(\frac{[M]^t}{\Delta t} - (1-\lambda)[ST]^{\Delta t} \right) \{c\}^t + \lambda \{F\}^{t+\Delta t} + (1-\lambda)\{F\}^t = 0 \tag{17}$$

where λ is the time-stepping weighting factor.

Pseudo-Lagrangian methods

In the pseudo-Lagrangian methods, the calculations are divided into two parts: the convection and the dispersion. The convective part in equation (6) is introduced by the following schemes:

(i) node moving with the fluid (FEM1)

(ii) backward interpolation (FEM2).

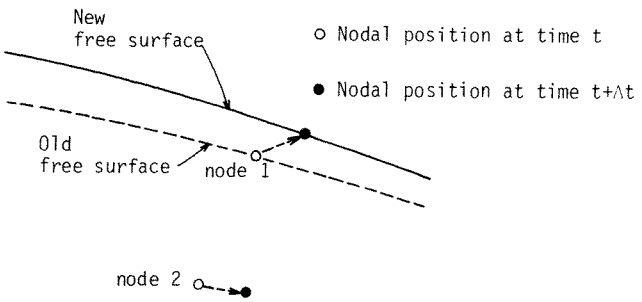

Figure 3. Typical moving nodes, FEM1

FEM1 (Lagrangian approach with moving mesh). In the first scheme the co-ordinates of each node are relocated simply by

$$x_i^{t+\Delta t} = x_i^t + u_i^{t+\Delta t}\,\Delta t \tag{18}$$

The scheme is diagrammatically shown in Figure 3 in which a typical node at the free surface is also shown.

A rising free surface coalesces the initial moisture content in the unsaturated zone thus forming a saturated front. In the case of θ_e, the effective porosity at the free surface, being smaller than θ_T, the Darcy porosity within the saturated zone, the tracer front will lag behind the saturated front. This phenomenon has been observed to be true in sandbox experiments.[3,14] According to the boundary condition (9) which implies instantaneous mixing at the free surface between resident fluid mixture and the incoming moisture, the mixing is realized by moving the nodes, which had been moved by the local velocity in the saturated flow, vertically to the free surface at the end of the timestep. The boundary condition is then applied when the dispersion part is solved.

The dispersion part is approximated by the non-linear heat conduction equation in Eulerian space

$$\frac{\partial c}{\partial t} = \frac{\partial}{\partial x_i} D'_{ij} \frac{\partial c}{\partial x_j} \tag{19}$$

This equation is solved using equation (17) with all u_i components set to zero. An explicit finite difference approximation is used in this case ($\lambda = 0$). This method eliminates numerical dispersion and produces only small numerical diffusion provided the movement of nodes is such that a well formed and appropriately graded mesh can be maintained. If the flow pattern is such that an overly distorted mesh results, rezoning must be carried out.

FEM2 (Lagrangian approach with stationary mesh). In the second scheme, as an extreme measure against the distortion of the mesh, a rigid mesh network is employed. However, nodal points at the free surface are allowed to move vertically with the free surface (see Figure 4). The convective part is introduced by retracing each node along its instantaneous pathline to a fictitious point of which co-ordinates ($x_i^{t-\Delta t}$) are determined by

$$x_i^{t-\Delta t} = x^t - u_i^t\,\Delta t \tag{20}$$

A concentration value at that point is then evaluated by interpolation. The convection is accomplished by transferring the concentration value from the fictitious point to the nodal point. Readers are referred to References 14 and 20 for more details.

At the free surface, convection is treated in a way similar to that in FEM1. Each node at the free surface is retraced in the x-direction by equation (20) and vertically moved to the

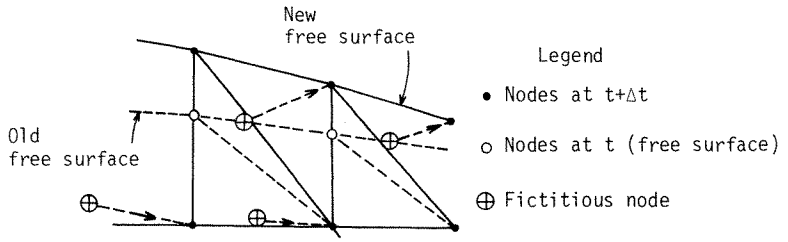

Figure 4. Typical FEM2 nodes

free surface at time $t-\Delta t$. The dispersion part is then solved in a manner identical to that of FEM1.

Eulerian methods

FEM3 (Eulerian approach with pseudo saturated–unsaturated domain. The most rigorous approach to the flow problem is to consider both saturated and unsaturated zones thus eliminating the free surface. In practice, however, if the saturated domain is much more significant than the unsaturated domain, a solution to the flow problem is normally sought through the saturated approach because of the significant difference in computational effort involved. The savings in computational effort are twofold. The permeability is independent of saturation and the flow equation is linear. Secondly, fine discretization in the neighbourhood of the saturated front (free surface) is not essential.

In this scheme the concept of the moving boundary is modified in the solution of the hydrodynamic dispersion equation. The unsaturated zone is also included in the domain of interest so that the moving free surface is eliminated. Because the solution to the flow equation is sought through the saturated flow theory, it is more convenient to employ two meshes (one for the flow and another for the transport equation) than to employ a single mesh with the free surface condition enforced by the Lagrangian multiplier method. Once the flow solution is obtained, the velocity distribution is mapped onto the transport mesh.

Velocity above the free surface is taken as zero everywhere except in the region under recharge sources where the vertical component is taken to be $-P_0/\theta_T$. A typical domain is shown in Figure 5 in which boundary conditions at the ground surface are also displayed. The solution of the transport equation is obtained by solving equation (17) with $\frac{1}{2} \leqslant \lambda \leqslant 1$.

FEM4 (Eulerian approach with non-stationary mesh). In this scheme the domain of interest is confined to the saturated zone. A typical discretization is shown diagrammatically in Figure 6. The discretization at time $t+\Delta t$ is superimposed on the one at time t. In this case the discretization is allowed to expand or contract to accommodate the non-stationary saturated domain. For a situation where there is no lateral movement of the saturated zone such as that in Figure 6, tracking of the mesh network is confined to the vertical direction only.

The process of time marching in this scheme is quite efficient because interpolation between timesteps of concentration at new node locations is not required.

The transport equation is transformed by the following transformation[3,14]

$$\xi_i = x_i - \frac{\partial x_i}{\partial t}\,\delta t = x_i - w_i\,\delta t$$

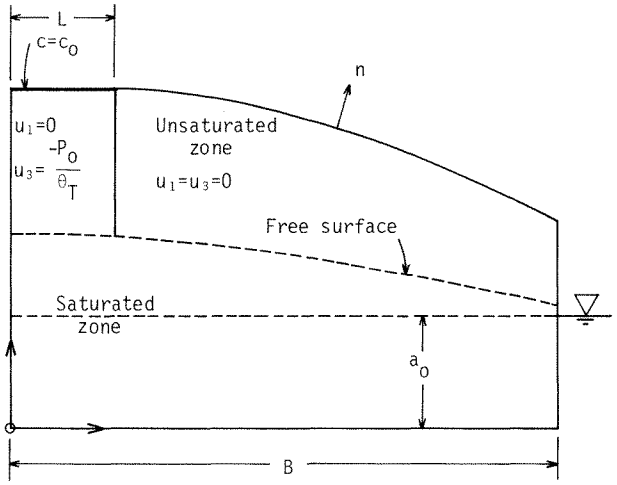

Figure 5. Pseudo saturated-unsaturated domain

with which equation (6) is rewritten as:[16]

$$\frac{\partial c}{\partial t}+(u_i-w_i)\frac{\partial c}{\partial \xi_i}=\frac{\partial}{\partial \xi_i}D'_{ij}\frac{\partial c}{\partial \xi_j} \tag{21}$$

where w_i is the relative velocity between the Cartesian reference frame x_i and the curvilinear reference frame ξ_i, and δt the time elapsed from time t.

The relative velocity w_i is approximated by $\Delta d_i/\Delta t$ where Δd_i is the movement of the centroid of each element between time t and $t+\Delta t$.

Equation (21) is solved using equation (17) by replacing u_i with u_i-w_i and x_i with ξ_i, respectively, and by setting $\lambda=\frac{1}{2}$. Guvanasen[14] and Guvanasen and Volker[3] give more details.

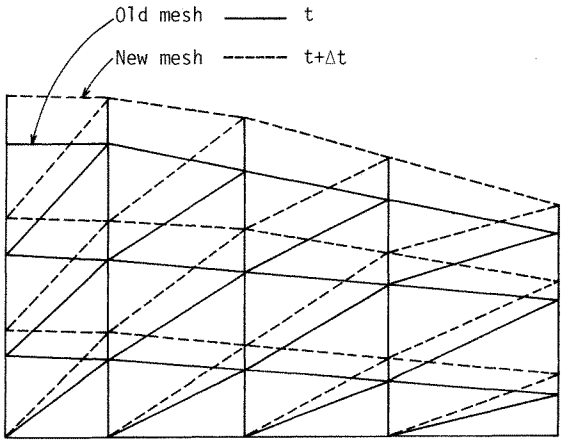

Figure 6. Non-stationary mesh in the saturated domain

RESULTS AND DISCUSSION

Numerical experiments for one-dimensional flow

In order to obtain a preliminary assessment of relative accuracies of the methods some numerical experiments are performed on a one-dimensional model and the results from the different methods are compared with a known analytical solution. Parameters employed in the comparison are the Peclet number and Courant number which are defined below:

$$\text{Peclet number} \quad Pe = u\,\Delta x/D$$

$$\text{Courant number} \quad Cr = u\,\Delta t/\Delta x$$

where Δx is the mesh size, u the velocity, D the coefficient of dispersion, and Δt the timestep.

Numerical models are subjected to the following initial and boundary conditions:

$$c = 0 \quad \text{at} \quad t = 0$$

$$c = c_0 \qquad x = 0$$

$$\frac{\partial c}{\partial x} = 0 \qquad x = B$$

The concentration profile, before the downstream boundary effect is felt, is given by:[17]

$$\frac{c}{c_0}(x, t) = \tfrac{1}{2}(\text{erfc}[(x - ut)/(4Dt)^{1/2}] + \exp(ux/D)[\text{erfc}\,(x + ut)/(4Dt)^{1/2}]) \tag{22}$$

where erfc is the complementary error function.

MOC. Experiments on one-dimensional MOC have been carried out by Garder *et al.*[7] and Reddell and Sunada.[8] Reddell and Sunada[8] experimented with $Cr = 0{\cdot}1$ to $1{\cdot}0$, $Pe = 2$ to 20, and found that the error for MOC behaved strangely and did not seem necessarily to get smaller with a smaller grid size. They concluded that it was due to the method used for calculating the average grid concentration and the relative positions of the moving point inside the grid. Since the most practical method of averaging concentration at a grid point is to use the simple arithmetic mean of concentration inside the cell, the only way of reaching convergence is through increasing the number of moving points. The lower limits of the number of points were reported by Garder *et al.*[7] and Reddell and Sunada[8] to be two and four, respectively. In the present study, at least four points per grid were employed.

From similar experiments for the work presented here with Cr varying from 0.25 to 1 and Pe from 10 to 100, it is found that Cr does not significantly affect the solution accuracy; however, for cases with large Pe the method suffers from numerical diffusion as shown in Figure 7.

FEM1. For uniform flow, Cr plays no important role since the mesh is not deformed. In non-uniform flow, Cr should be kept below unity so as to minimize truncation error in nodal relocation.

The resultant heat equation is solved by an explicit scheme. It is found that the lumped mass matrix[18] (M in equation (17)) gives better numerical stability than does the consistent one.[18] For a uniform mesh, the numerical stability can be derived by the use of the von Neumann's method to give:

$D\,\Delta t/\Delta x^2 < \frac{1}{6}$, consistent mass matrix; and

$D\,\Delta t/\Delta x^2 < \frac{1}{2}$, lumped mass matrix.

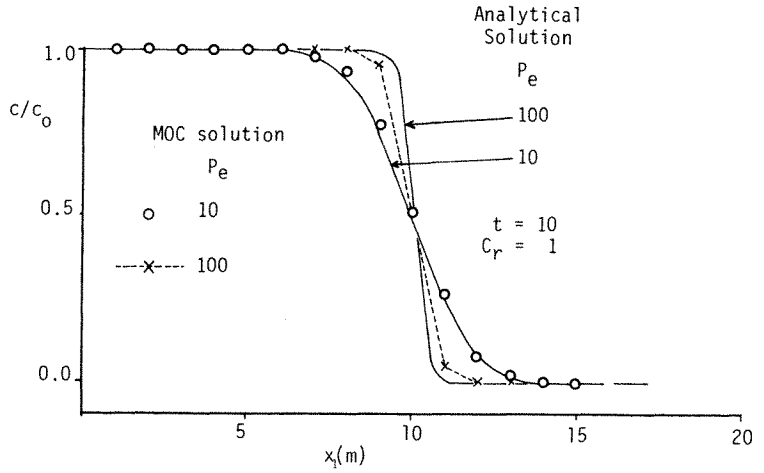

Figure 7. Comparison of analytical and MOC concentration profiles with varying *Pe*

Therefore unless *D* is abnormally large, an explicit scheme with lumped mass matrix may be economically employed.

Figure 8 shows results from cases with varying *Pe*. It is obvious that spurious oscillation is absent. For large *Pe*, however, steep concentration gradients can no longer be represented by discrete nodes and flatter gradients result due to numerical diffusion.

FEM2. Because the solution procedure for the heat equation is identical to that of FEM1, the lumped mass matrix is also employed in this scheme. It is evident from Figure 9 that the quality of the solution depends largely on the value of *Pe*. Numerical diffusion becomes more obvious as *Pe* increases. The impact of *Cr* is less apparent as shown in Figure 9. A small *Cr* introduces more numerical dissipation due to the larger number of interpolations carried out. In general *Cr* lies between 0 and 1, and *Pe* should be used as a criterion.

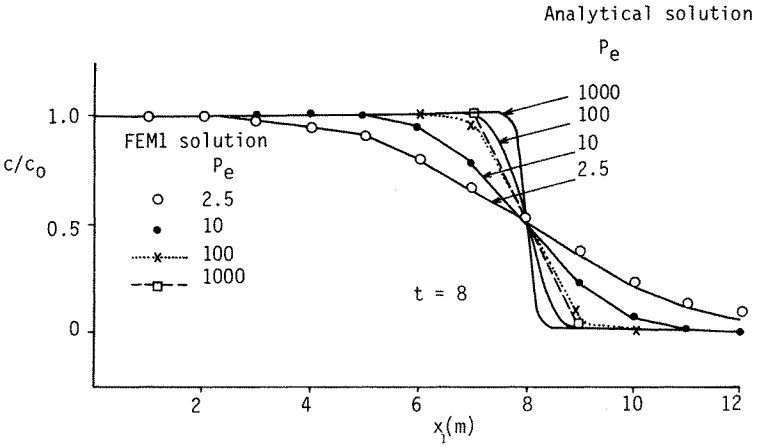

Figure 8. Comparison of analytical and FEM1 concentration profiles with varying *Pe*

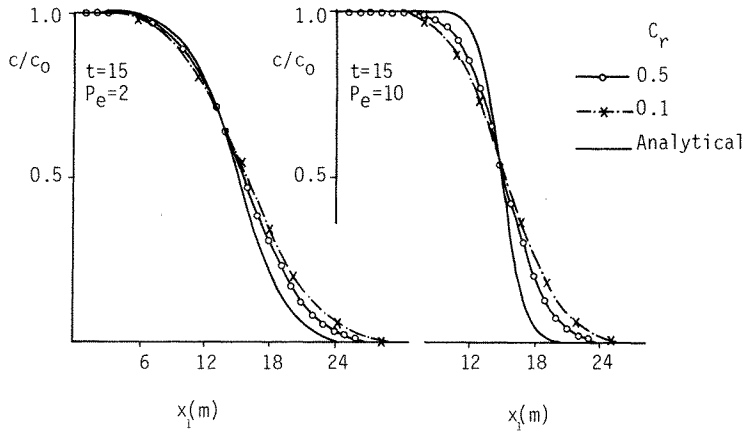

Figure 9. Comparison of analytical and FEM2 concentration profiles with varying Pe and *Cr*

FEM3. Experiments performed on the Eulerian scheme using Galerkin's technique indicate that the accuracy of the solution is affected by both *Cr* and *Pe*. Figure 10(a) shows that oscillation occurs as *Pe* is increased although the accuracy is improved when *Cr* is decreased as shown in Figure 10(b). If slight numerical dispersion can be tolerated ($\leqslant$5 per cent), then $Pe \leqslant 40$, and $Cr \leqslant 0{\cdot}5$ can be used as criteria for acceptable accuracy. Since Pinder and Gray[19] found that the consistent mass matrix is superior to the lumped mass matrix, the consistent mass matrix is employed throughout this solution scheme.

FEM4. The concept of the non-stationary mesh in the Eulerian scheme is also tested in a hypothetical situation in which the domain expands with time. As shown in Figure 11(a), the edge of the domain on the right-hand-side moves at a speed 4 times greater than that of the field velocity, which in turn causes the discretization inside the domain to expand to accommodate the new domain. The left-hand-side of the domain remains stationary at all

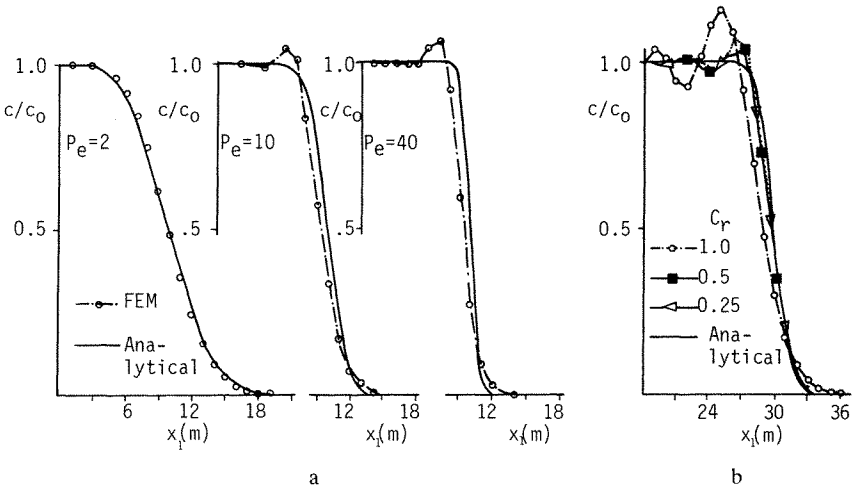

Figure 10. (a) Comparison of analytical and FEM3 concentration profiles with varying *Pe* for $C_r = 1$ at $t = 10$. (b). Comparison of analytical and FEM3 concentration profiles with varying *Cr* for $Pe = 40$ at $t = 30$

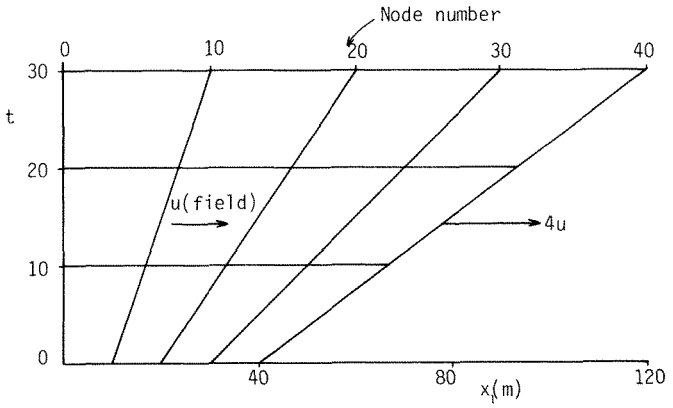

Figure 11(a). Mesh layout for FEM4

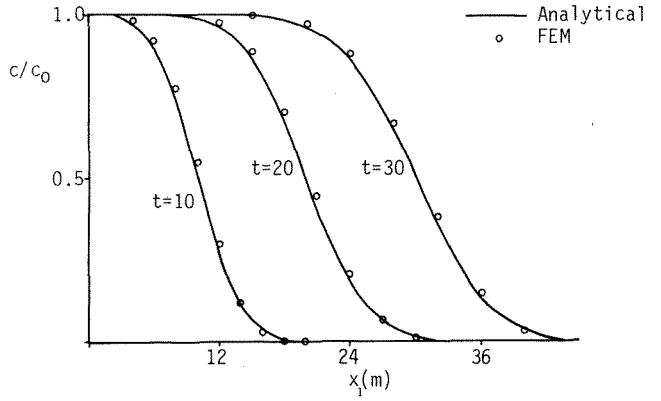

Figure 11(b). Concentration profiles from FEM4 for $u = 1$, $\Delta t = 0{\cdot}25$, $D = 0{\cdot}5$

times and the boundary condition at that point is $c(0, t) = c_0$. An approximate analytical solution to this particular problem is given by equation (22).

A comparison between the analytical and numerical solutions is made in Figure 11(b) from which it is evident that the numerical solution agrees quite well with the analytical solution. It should be noted that resolution of the mesh is impaired as the domain expands. This problem can be overcome by assigning adequate numbers of nodes for the maximum expected domain size. Since not all elements are moving at the same speed, *Pe* and *Cr* vary from element to element and results from FEM3 experiments may be employed as criteria. Because of the similarity between this scheme and FEM3, the consistent mass matrix is also employed.

Two-dimensional models

Comparison between MOC and FEM1. Results from numerical simulation of unsteady flow in unconfined aquifers indicate that FDM is less efficient than FEM. Since MOC is dependent on the FDM solution, it is necessary to assess the performance of the MOC independently prior to its coupling with the FDM unsteady flow solution. This is accomplished by first comparing it with FEM1, using a steady state flow field of the configuration

Table I. Physical properties

Case	K (m/s)	L (m)	a_0 (m)	B (m)	θ_e	θ_T	a_1	a_2	n_1	n_2	d_{50} (m)	P_0 (m/s)
1	5×10^{-3}	35	27	300	0·375	0·375	0·66	0·036	1	1	9×10^{-4}	$1{\cdot}236\times10^{-4}$
2	$1{\cdot}72\times10^{-2}$	0·30	0·16	6	0·325	0·491	1·75	0·073	1·22	0·693	$1{\cdot}8\times10^{-3}$	$1{\cdot}009\times10^{-3}$

1. Assumed values for case 1
2. Experimentally determined values for case 2
3. L, a_0, B are geometrically defined in Figure 1
4. a_1, a_2, n_1, n_2 are used for calculation of D'_{ij}—see Appendix for details.

shown in Figure 1. Boundary conditions are given by equations (7), (8) and (9) with $\partial h/\partial t = 0$. It is also assumed that there is no diffusion or dispersion from the bottom of the basin to the free surface so that the influent solute concentration at the free surface is equal to the concentration in the strip basin above.

Taking advantage of symmetry, only one half is considered. Related physical properties are given in Table I, case 1. The coefficients of dispersion are chosen to be small so as to observe the performance of each model under the sharp front condition.

In MOC, the recharge boundary is treated by assuming that each point represents a definite area (or volume) of fluid which is equal to $(\Delta x)^2$/(number of points in each square grid), Δx being the grid interval. In each time step a layer of invading fluid is deposited at the free surface underneath the recharge or disposal pit. The number of points in each layer is arranged so that the area (or volume) they represent is equal to $LP_0\,\Delta t/\theta_T$, P_0 being the infiltration rate.

In FEM1, the recharge boundary is treated by introducing new elements at the boundary. The frequency, at which the inclusion of the new elements takes place, varies depending on the proximity of the front to the boundary (every 1, 2 or 3 time steps etc.).

In order to maintain an identical velocity distribution pattern for all time steps, two sets of mesh are employed in FEM1: one for the flow equation and the other for the transport equation. In each time step spatially dependent velocities for each node in the transport mesh are calculated from the head distribution in the flow mesh. The models (MOC and FEM1) are run for several discretization conditions, the details of which are presented in Tables II and III.

Vertical concentration profiles at $x = 10$ m are plotted in Figure 12. All cases yield approximately the same position of $c/c_0 = 0{\cdot}5$ and in no case is numerical dispersion observed. Because concentration profiles from all FEM1 cases are almost indistinguishable only one curve is used to represent the results.

Inspection of Figure 12 and Tables II and III shows that as Δx decreases (Pe decreases) solutions of MOC approach that of FEM1 whose mesh can be economically graded to

Table II. Discretization details of MOC

Case	Δx_1 (m)	Δt (s)	Total number of Δt	Number of points per cell	Number of injected points/layer/Δx	CPU* (s)
1	10	7582	20	16	4	30·0
2	5	3791	40	16	4	103·7
3	2·5	1895·5	80	16	4	435·17

* Performed on the DEC-system 10 at the James Cook University of North Queensland.

Table III. Discretization details for FEM1

Case	Flow model: Number of nodes	Flow model: Number of elements	Transport model: Number of nodes	Transport model: Number of elements	Δt (s)	CPU* (s)
1	36	48	24–48†	28–60†	7582	23·12
2	102	160	95–135†	144–208†	7582	82·95
3	102	160	95–135†	144–208†	3791	137·22

* Performed on the DEC-system 10 at the James Cook University of North Queensland.
† The first value is the initial number, the second value is the final number.

accommodate steep gradient conditions. Improvement in accuracy and resolution in MOC can be done at the expense of computing cost as shown in Tables II and III.

Concentration contours from both schemes (case 3, MOC and case 3, FEM1) are shown in Figure 13. Good agreement is observed everywhere except in the vicinity of the free surface. One explanation for such an occurrence is that the approach to the solution of the flow equation in the vicinity of the free surface is different, thereby affecting the velocity magnitudes which are calculated from head values in this region. Owing to the fact that MOC tends to incur prohibitive computational cost, it was not compared with other schemes.

Comparison of finite element models. Since each finite element scheme for the transport equation employs a different discretization, only one flow model is used. This is to provide identical patterns of velocity for each scheme so that each scheme is assessed on its own merit. The performance of the models is demonstrated through a problem shown in Figure 1 for which data from sandbox experiments are available.[14] Before the introduction of solute infiltration, the water table is horizontal and the water level is equal to that in the side drains. The boundary conditions are given by equations (7), (8) and (9). Following the argument given earlier (in comparison between MOC and FEM1) it is assumed that the influent solute concentration at the free surface is equal to that in the recharge basin above. Because of the symmetry of the problem, only one half need be considered. Physical properties of the aquifer are given in Table I, case 2. Temporal and spatial discretizations are presented in Table IV. In FEM1 it is assumed that the boundary condition at the downstream end does not significantly affect the conditions upstream so that only a small portion of the domain need be covered by a finite element mesh. The number of nodes and elements may therefore

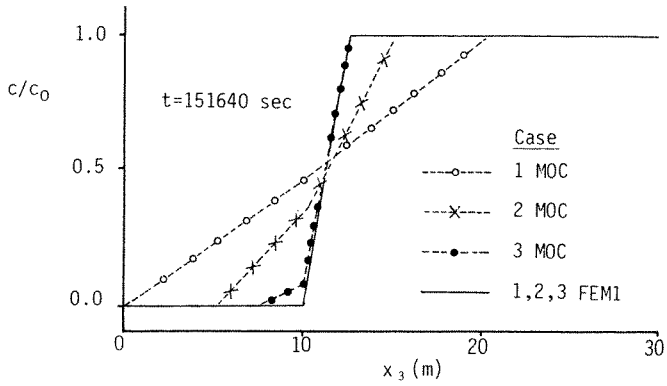

Figure 12. Comparison of concentration profiles from MOC and FEM1 for Case 1 in Table I ($x_1 = 10$ m, $0 < x_3 < 30$ m)

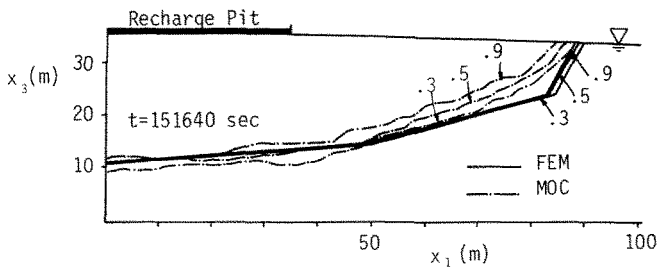

Figure 13. Comparison of concentration contours between MOC case 3 (Table II) and FEM1 Case 3 (Table III)

vary to cover different sizes of domain. In FEM3, the number of nodes and elements is largest because the unsaturated zone above the water table must also be covered.

It has been shown in the one-dimensional problem that the desired accuracy may be achieved by appropriate discretizations. In this particular problem, if slight oscillation at the front is tolerated the discretizations employed should enable FEM3 and FEM4 to predict fairly accurately the position of the front. Conditions of the discretization employed are $Pe \leq 40$ (approx.), $Cr \leq 0{\cdot}4$ (approx.).

The performance of the above four schemes is tabulated in Table IV in the form of CPU/timestep and CPU/timestep/element; the former is to indicate the overall performance of the scheme and the latter to determine the efficiency at elemental level. It is evident that FEM3 is the most efficient in terms of CPU/timestep/element. This is because velocities and

Table IV. Discretization details of FEM Schemes

Flow model

	Number of nodes	Number of elements
Coarse mesh	144	210
Fine mesh*	287	480

Hydrodynamic dispersion model

Scheme	Number of nodes	Number of elements	CPU/time step† (s)	CPU/time step/ element† (s)
FEM1	30–120‡	40–184‡	4·39–20·21‡	0·11
FEM2	180	280	17·02	0·061
FEM3	410	720	11·06	0·015
FEM4	205	320	8·03	0·025
FEM4* (fine mesh)	287	480	12·97	0·027

For the flow model $\Delta t = \frac{1}{6}\Delta t_i$ where Δt_i for the convective-dispersion model is:

$$\Delta t_i = 1{\cdot}01\,\Delta t_{i-1} \leq 4\Delta t_0 \quad \text{and} \quad \Delta t_0 = 24\text{ s for all schemes.}$$

* The same mesh for flow and hydrodynamic dispersion models.
† Performed on the DEC-system 10 at the James Cook University of North Queensland.
‡ The first value is the intial number, the second value is the final number.

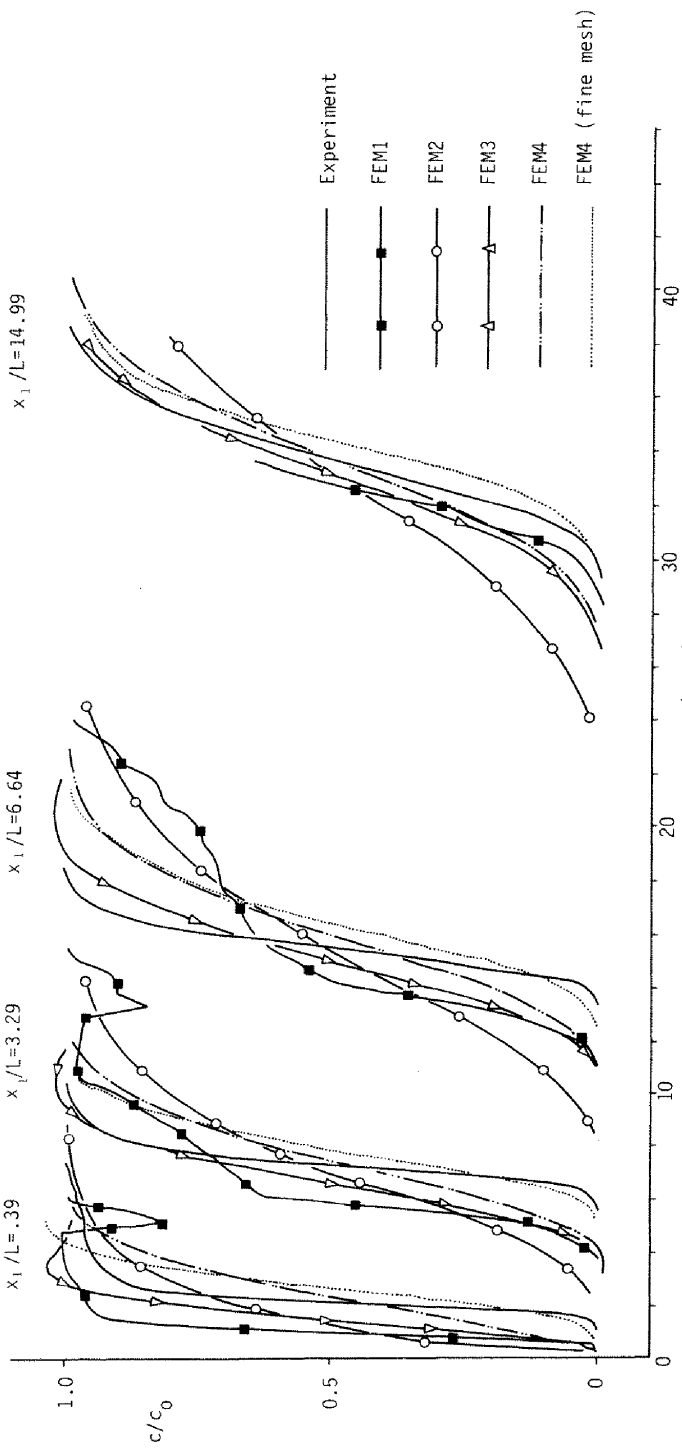

Figure 14. Comparison of experimental and FEM breakthrough curves at $x_3/a_0 = 0{\cdot}33$

convective dispersion coefficients are assumed to be zero in the inactive unsaturated area. At the elemental level, FEM1 appears to be the least efficient because of the necessity to occasionally rezone the overdistorted mesh and to relocate all nodes in every timestep.

On an overall performance basis, FEM1 does well initially when the number of nodes and elements is small and mesh rezoning has not taken place. The scheme decreases in efficiency when the number of elements increases and mesh deformation occurs. FEM4 appears to be the most economical overall because its CPU/timestep is lowest. As a check for convergence a case with refined discretization is included. Since FEBM4 is the most economical scheme, it is therefore selected for the test with finer discretization. In this case the same mesh is used for both flow and transport solutions.

Breakthrough curves from all FEM schemes (including FEM4 with a fine mesh) are compared with the experimental data in Figure 14. It can be seen that calculated arrival times at various locations agree well with the experimental data. The correspondence between the data and calculation is only marginally improved when the finer discretization is employed for FEM4.

$c/c_0 = 0{\cdot}5$ contours from various schemes are shown in Figure 15. Comparison of results from all schemes using identical flow models indicates that the contours are close to each other and the discrepancy between them is quite negligible considering the extent of the domain of interest. Furthermore, one-to-one correspondence cannot be ensured because of different discretizations employed and slight discrepancies in the convective magnitude are therefore unavoidable. Comparison between the contours of FEM4 (fine mesh) and the others reveals that at an early stage when the front is under the basin the former lags slightly behind the latter ones due to the differences in the flow patterns. As the front moves away from the basin they appear to be in approximately the same position. Generally, differences between results from fine and coarse discretizations are considered insignificant compared to the extent of the domain.

Relative front widths for all schemes are also exhibited in Figure 15. FEM2 shows the largest width and FEM1 the smallest. An inspection of Figure 14 reveals that when $tP_0/(a_0\theta_T) = 5{\cdot}69$ ($t = 1033$ s), FEM1 still preserves the gradient of breakthrough curves suggesting that the front width predicted by FEM1 at that time is approximately correct. Note that major smearing of breakthrough curves due to rezoning occurs after $tP_0/(a_0\theta_T) = 6{\cdot}2$ ($t = 1125$ s). For this reason, one may therefore employ FEM1 as a standard with which other schemes may be compared for the results shown in Figure 15. These results indicate that FEM2 suffers most from smearing whereas FEM3 and FEM4 experience approximately the same degree of smearing but less than that of FEM2. The front width of FEM4 (fine mesh) is smaller than that of FEM4 (coarse mesh) indicating that smearing can be attenuated by the use of a finer discretization; the values of CPU/time step in Table IV indicate the increased computational effort involved.

Discussion

Results from one-dimensional experiments show that numerical diffusion occurs with all schemes at large *Pe* and that *Cr* has a marked effect on accuracy in Eulerian FEM schemes but is less important in MOC and Lagrangian FEM.

From the two-dimensional flow cases, MOC does not compare favourably with FEM schemes in terms of computational economy and the ease with which boundary conditions can be incorporated at the free surface. In addition the FDM flow equation solution is more expensive than its FEM counterparts[6] and for these reasons, MOC is not considered competitive for the particular problem studied.

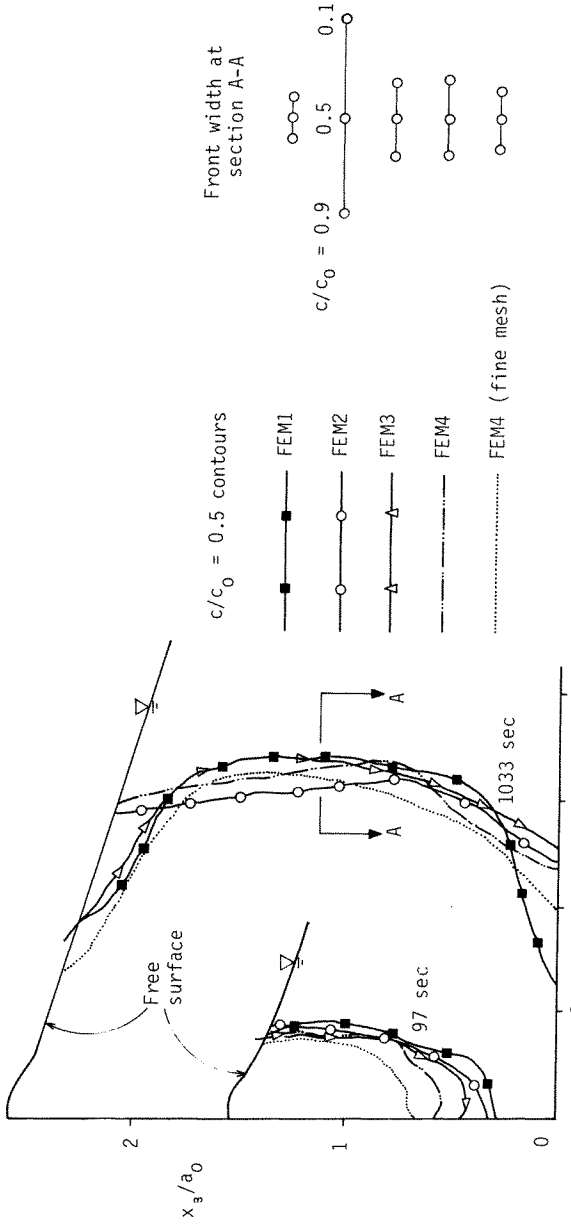

Figure 15. Comparison of calculated $c/c_0 = 0{\cdot}5$ contours and front widths for all FEM schemes

An examination of Figures 14 and 15 reveals that problems with FEM schemes include smearing of the front due to rezoning (FEM1), smearing of the front due to interpolation truncation error (FEM2), and numerical dispersion and diffusion (FEM3 and FEM4).

The selection of a scheme is generally dependent upon the type of problem to be solved. FEM1 has been demonstrated to be efficient only in the early stages, when the number of nodes and elements is small, as the processing time per element is relatively high. Work carried out by Sato and Thompson[13] also indicates that as the free surface approaches steady state the scheme is no longer economical. Furthermore, resolution in the solution is dependent upon rezoning schemes. In view of the above and other problems mentioned earlier, this scheme is only recommended for linear problems in which the flow domain is geometrically simple, the flow pattern uncomplicated, and the area needed to be covered by the transport model is small compared to that required for the flow model.

Adey and Brebbia[20] indicated that an FEM scheme similar to FEM2 reduced the storage requirement by one half and CPU time by two thirds compared with an iterative Eulerian scheme. Results from this study indicate that FEM2 is less efficient than the weighted time-stepping Eulerian schemes and furthermore, accuracy is limited to small values of *Pe*. In other words, numerical dispersion is eliminated at the expense of smearing of the front. Numerical dispersion and diffusion in FEM3 and FEM4 may be alleviated using upwind weighting functions.[12] At high values of *Pe* such a reduction of the numerical oscillation leads to smearing at the front.[19]

Based on considerations of computational efficiency and accuracy for long-term contaminant transport problems the Eulerian approaches (FEM3, FEM4) appear to be better than their pseudo-Lagrangian counterparts (FEM1, FEM2).

The results in Table IV for CPU time per time step (since the time step is identical in all cases) show that FEM4 is the most economical at longer times. It is also convenient to apply since only mesh is required.

CONCLUSIONS

Five numerical schemes (one MOC and four FEM) for solving the problem of solute transport in unsteady flow in unconfined aquifers are compared using experiments on one and two-dimensional flow cases. The results for one-dimensional flow indicate that the accuracy is strongly dependent upon discretization especially at high mesh Peclet numbers. For two-dimensional cases the finite element schemes are found to be more computationally economical than MOC. The finite element scheme that is considered most efficient overall is the one with Eulerian formulation which allows the elements to expand or contract to accommodate the non-stationary saturated domain without any intermediate interpolation.

APPENDIX. CALCULATION OF DISPERSION COEFFICIENTS

The tensor D'_{ij} is calculated from the formula

$$D'_{ij} = D_T \delta_{ij} + (D_L - D_T) \frac{u_i u_j}{U^2}$$

where D_L is the longitudinal coefficient of dispersion, D_T the lateral coefficient of dispersion, and U the magnitude of local pore velocity.

D_L and D_T are estimated by[21]

$$D_L = va_1 Re^{n_1}$$

$$D_T = va_2 Re^{n_2}$$

$$Re = \text{Reynolds number} = d_{50}\, U/v$$

where v is the kinematic viscosity of water ($1{\cdot}011 \times 10^{-6}$ m^2/s in this study), d_{50} the 50 per cent finer diameter of the porous medium, a_1 and a_2 the experimentally determined dispersivity constants, n_1 and n_2 experimentally determined exponents.

REFERENCES

1. G. Segol, 'A three-dimensional Galerkin finite-element model for the analysis of contaminant transport in saturated-unsaturated porous media', *Proc. 1st Int. Conf. on Finite Elements in Water Resour.*, Princeton Univ., July, 1976.
2. J. F. Pickens and W. C. Lennox, 'Numerical simulation of waste movement in steady groundwater flow systems', *Water Resour. Res.*, **12** (2), 171–190 (1976).
3. V. Guvanasen and R. E. Volker, 'Simulating mass transport in unconfined aquifers', *ASCE J. Hydraul. Div.*, **107** (HY4), 461–477 (1981).
4. C. J. Taylor, P. W. France and O. C. Zienkiewicz, 'Some free surface transient flow problems of seepage and irrotational flow', in J. R. Whiteman (Ed.) *Mathematics of Finite Elements and Applications*, Academic Press, New York, 1971, pp. 313–326.
5. S. P. Neuman and P. A. Witherspoon, 'Finite element method of analyzing steady seepage with a free surface', *Water Resour. Res.*, **6** (3), 889–897 (1970).
6. V. Guvansen and R. E. Volker, 'Numerical solutions for unsteady flow in unconfined aquifers', *Int. J. Num. Meth. Eng.*, **15,** 1643–1657 (1980).
7. A. O. Garder, P. W. Peaceman and A. L. Pozzi, 'Numerical calculation of multidimensional miscible displacement by the method of characteristics', *AIME Soc. Pet. Eng. J.*, **4,** 26–36 (1964).
8. D. L. Reddell and D. K. Sunada, 'Numerical simulation of dispersion in groundwater aquifers', *Colo. State Univ. Hydrol. Pap.* **41,** 79 pp. (1970).
9. D. B. Spalding, 'A novel finite-difference formulation for differential expressions involving both first and second derivatives', *Int. J. Num. Meth. Eng.*, **4,** 541–550 (1972).
10. D. L. Book, J. P. Boris and R. Hain, 'Flux-corrected transport II: generalization of the method', *J. Comput. Phys.*, **18,** 248–283 (1975).
11. D. C. L. Lam, 'Comparison of finite element and finite difference methods for nearshore advection-diffusion transport models', *Proc. 1st Int. Conf. on Finite Elements in Water Resour., Princeton Univ.*, July, 1976.
12. J. C. Heinrich, P. S. Huyakorn and O. C. Zienkiewicz, 'An "upwind" finite element scheme for two-dimensional convective transport equation', *Int. J. Num. Meth. Eng.*, **11,** (1977).
13. A. Sato and E. Thompson, 'Finite element models for creeping convection', *J. Comput. Phys.*, **22** (2), 229–244 (1976).
14. V. Guvanasen, 'Theoretical and experimental studies of clogging and contamination in artificial groundwater recharge', *Ph.D. thesis, James Cook Univ.*, Townsville, Australia, 352 pp (1979).
15. J. Bear, *Dynamics of Fluids in Porous Media*, Elsevier, New York, 1972.
16. B. M. Mollowney, 'Solutions of the advective-diffusion equation by the method of moving coordinate systems with particular reference to the modelling of estuarine pollution', in C. A. Brebbia (Ed.) *Mathematical Models for Environmental Problems*, Pentech Press, London, 1976, pp. 313–327.
17. A. Ogata and R. B. Banks, 'A solution of the differential equation of longitudinal dispersion in porous media', *Paper 411–4, U.S. Geol. Survey*, 7 pp (1961).
18. O. C. Zienkiewicz, *The Finite Element Method*, 3rd edn., McGraw-Hill, London, 1977.
19. G. F. Pinder and W. G. Gray, *Finite Element Simulation in Surface and Subsurface hydrology*, Academic Press, New York, 1977.
20. R. Adey and C. A. Brebbia, 'Finite element solution for effluent dispersion', in C. A. Brebbia and J. J. Connor (Eds.) *Numerical Methods in Fluid Dynamics*, Pentech Press, London, 1974, pp. 325–354.
21. D. R. F. Harleman and R. R. Rumer, 'Longitudinal and lateral dispersion in isotropic porous medium', *J. Fluid Mech.*, **6,** (3), 385–394 (1963).